euronoise

High-frequency broadband acoustic current tomography in shallow water

Jing Luo[a], Entin Karjadi[b] and Mohsen Badiey[a]

[a]University of Delaware, College of Marine and Earth Studies, S. College Street, Newark, DE 19716, USA
[b]College of Marine and Earth Studies, University of Delaware, Newark, DE 19716, USA
badiey@udel.edu

Abstract: To study current tomography in very shallow water regions, a simultaneous oceanographic and broadband (1-25 kHz) acoustic experiment was conducted in Delaware Bay. The mean water depth was 15 m and the source-receiver range was 387 m. In this paper, the feasibility of using reciprocal acoustic transmission for current tomography applications is discussed. A beamforming technique is used to resolve the arrival time of direct and surface bounce rays since in shallow water the received acoustic signals are more complicated due to multiple interactions with bottom and sea surface. The current velocity prediction results are compared with ADCP measurements to determine the feasibility of current tomography in shallow water.

1 Introduction

Ocean acoustic tomography is now widely accepted as a powerful tool for monitoring the variability in marine environment. Methods for ocean acoustic tomography [1, 2] have been applied mostly for ocean scenarios where the water depth and source-receiver range allowed acoustic multi-paths to be independently resolved and separated. However, in very shallow water, due to a strong acoustic signal interaction with sea surface and bottom, the separation of arrivals which correspond to different ray paths is more difficult, demanding acoustic transmissions with high frequencies and large bandwidth. High-frequency signals, however, can lack of the coherence [3] and regularity necessary to interpret the received signals.

The objective of this paper is to examine the feasibility of current tomography in shallow water using high frequency broadband acoustic transmission. The data used in the study are from the measurements of reciprocal high frequency acoustic transmission and oceanographic parameters in Delaware Bay in 1997 [3]. The current velocity is estimated by differencing the arrival time of reciprocal signals from direct and surface bounce ray paths from a common clock. The effects of center frequency and bandwidth as well as the effects of environmental conditions on the current velocity estimation are shown.

2 Experimental observations

A high frequency acoustic experiment (HFA97) [3] was conducted from September 22 to 29, 1997 in the middle of Delaware Bay region shown in Fig. 1. The average water depth was approximately 15 m. During the experiment, both acoustic and environment data were collected simultaneously. The acoustic source and receiver were co-located on stable tripods and were self-contained, separated from the research ship, providing continuous measurements for the entire experiment.

2.1 Environmental measurements

Environmental variations have strong impact on the acoustic signal propagation. To assess the acoustic signal correlation with the environmental fluctuations, variety of environmental parameters were measured simultaneously, which include salinity and temperature profiles using a shipboard Conductivity Temperature Depth (CTD), dynamic water pressure near sea bottom and video images of the sea surface. The air temperature, wind speed and direction at different points above the sea surface were also measured. In addition, the vertical current profile was measured at one point between the acoustic source-receiver pair using Acoustic Doppler Current Profiler (ADCP). The accurate measurements of the current are important in understanding both the dynamics of the bay and the current effects on the propagation of the acoustic signals.

Fig. 1: Map of the Delaware Bay. The location of the high frequency acoustic and oceanography experiments is marked in as experiment site.

In Fig. 2, a set of the environmental data for the entire HFA97 experiment is plotted. Figure 2(a) shows the wind speed and direction and Fig. 2(b) shows the tide height data. During the week of the experiment, the wind speed varies from less than 1 m/s to around 15 m/s hence provide conditions to study the effects of sea surface roughness. Figure 2(c) shows the vertical current profile which was projected along the acoustic propagation path with positive direction into the bay. Figure 2(d) shows the sound speed profile obtained from MacKenzie empirical approximation [4] using CTD salinity and temperature profile. The current is clearly dominated by the 12-hour tidal constituents. Therefore the dominant effect of the current on the acoustic signal propagations will be due to tidally induced changes in the sound speed within the water column. Note that there is more stratification on the sound speed during the ebb-tide and the period of slack-tide immediately following. Vertical mixing effects are stronger during flood-tide, when the tidal currents oppose the outflow from the river, and this reduces or eliminates the vertical sound speed gradients.

The current also directly affects the travel time of the acoustic signals. In general, the travel time will be longer when the signals propagate against the current and will be shorter when propagating with the current.

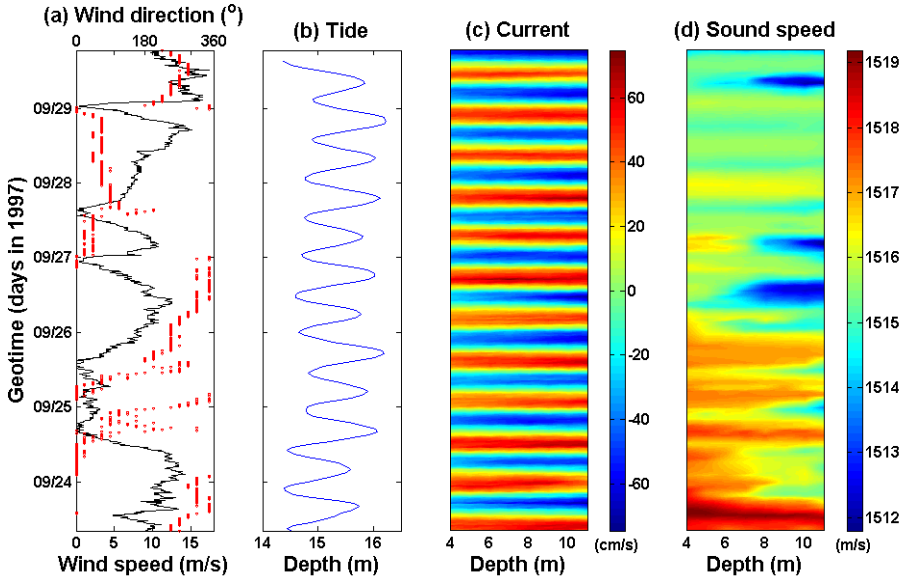

Fig. 2: (a) Measured wind speed and direction for HFA97; (b) Tide height; (c) Current measured with an ADCP; (d) Sound speed profile obtained from CTD measurements of temperature and salinity profiles using MacKenzie empirical approximation. Note: Depth (m) on (b), (c), and (d) is measured from the sea floor.

2.2 Acoustic measurements

During the HFA97 experiment, a reciprocal acoustic transmission experiment was conducted using two pairs of source-receiver arrays mounted on tripods A and C connected by underwater electrical cables to a central computer. The source and receiver had been successfully synchronized, therefore the same time reference was established for all the transmitted and received signals.

In each source-receiver unit the acoustic source was mounted on top of the tripod at 3.125 m above the seafloor, and three hydrophones were mounted at 0.33 m, 1.33 m and 2.18 m above the seafloor respectively. The distance between the two tripods was 387 m measured directly from Differential Global Positioning System (DGPS) at the time of deployment. This distance was set to ensure the separation of the direct acoustic ray path from the boundary ray paths that arrived later.

The energy following different ray paths arrives at the receiver in groups. Figure 3 shows the first two ray groups in the experiment. The first group includes direct (D) and single bottom bounce (B) rays with no surface interaction. The second group is four rays with single surface interaction, i.e. surface (S), surface-bottom (SB), bottom-surface (BS), and bottom-surface-bottom (BSB) rays. By performing simple ray calculations, it can be shown that rays having the same number of surface interactions have very close travel distances. Hence these rays may interfere with each other and arrive at the receiver in a group.

In the experiment, the source transmitted linear chirp signals from 1 to 25 kHz. The broad frequency band provided the acoustic resolution to resolve micro- or macro-structures with spatial variability ranging from several centimeters to a few meters. The pulse length of the transmitted signal is 0.3495 s. The signals were transmitted using two different sampling durations, the short geotime and the long geotime, to capture the fast and slow temporal variations of the acoustic fields respectively. The short geotime signals (40 s duration) were transmitted from hydrophone A to C every hour, whereas the long geotime signals (5 s duration) were transmitted every 10 minutes from both hydrophones A to C and C to A with 3 s silence in between.

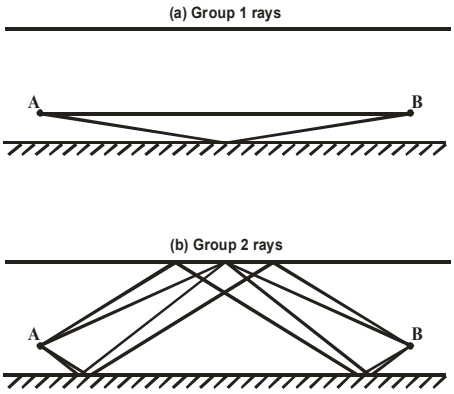

Fig. 3: Representation of the different groups of arrival.
(a) Group 1 includes paths with no surface interaction.
(b) Group 2 includes paths with single surface interaction.

3 Effects of signal center frequency, bandwidth, and sea surface condition

The acoustic ray signatures are strongly affected by the signal frequency and bandwidth [3]. To show the effects of center frequency and bandwidth Fig. 4 plots the received signal amplitude versus arrival time for center frequency 12 kHz with a bandwidth of 12 kHz (frequency 12-12 kHz) and center frequency 4 kHz with a bandwidth of 4 kHz (frequency 4-4 kHz) for 30 hr geotime starting at 5:00 on September 24, 1997. Five distinct groups of peaks are shown in this figure. It is clear that the first group arrival is much stronger at frequency 12-12 kHz than it is at frequency 4-4 kHz. This is due to the fact that at lower

center frequencies the phase difference between the direct and the bottom bounce rays in the first group has stronger effect on the ray interactions. For the later arrivals, a reverse phenomenon is observed. At a high center frequency, the later arrival signals are highly attenuated due to the fact that the scales of sea surface roughness accentuate non-specular scattering at short wavelengths.

The accuracy of current estimation depends mainly on the accuracy of peak arrival time measured from the acoustic data. As discussed above, the choice of the center frequency and bandwidth is critical to accurately measure the arrival time of each group.

In addition to the acoustic signal dependency on the center frequency and bandwidth, there is also a strong dependency on the ocean environmental variability. The weather condition changed dramatically during the one week of the experiment. The sea surface experienced calm and rough periods, so the collected acoustic data will allow us to examine the sea state effects on the acoustic transmission. The 30 hours period shown in Fig. 4 was chosen to show the transition between high to calm wind speed. At higher wind speed in the first 10 hours [see Fig. 3(a) for wind speed], the later arrivals which correspond to all ray paths with surface interaction are broken down randomly, while after hour 10 at a lower wind speed the acoustic data show peaks distinguished in groups.

4 Shallow water current tomography

A broadband acoustic remote sensing technique has been developed to measure travel times associated with reciprocal source-receiver pairs. This is a well established tomography technique which has been used in deep water [1]. Given the measured travel times and distances between source-receiver pair, range-averaged sound speed can be obtained and the spatially integrated current can be estimated.

4.1 Methodology

The travel time of eigenrays in a moving, range-independent ocean can be written as [1]:

$$t_n^{\pm} = \int_{\Gamma_n^{\pm}} \frac{ds}{C(z) \pm u(z)\cos(\theta)} \qquad (1)$$

where ± indicates a transmission in the positive/negative propagation direction. $C(z)$ and $u(z)$ are the depth dependent sound speed and current velocity, s is curve along the path Γ_n, and θ is the grazing angle of the ray path. A transceiver (source and receiver) is located at both the starting point and end point. The paths of integration $\Gamma^{\pm}$ are along the trajectories of the n^{th} ray and are generally functions of $C(z)$ and $u(z)$. The path geometry is reciprocal to order $u/C << 1$, therefore $\Gamma^{+} \approx \Gamma^{-} \equiv \Gamma$.

In a weak range-dependent shallow water environment, the average current velocity can be approximated as

$$u = \frac{C|t_{CA} - t_{AC}|}{(t_{AC} + t_{CA})\cos\theta} - \frac{|\Delta d|}{(t_{AC} + t_{CA})\cos\theta} \qquad (2)$$

or

$$u = \frac{2d|t_{CA} - t_{AC}|}{(t_{AC} + t_{CA})^2\cos\theta} - \frac{|\Delta d|}{(t_{AC} + t_{CA})\cos\theta} \qquad (3)$$

where Δd is the range offset from A to C and C to A due to equipment placement [5], t_{AC} and t_{CA} are the reciprocal transmission arrival time, and d is the source-receiver range. In the HFA97 experiment, the distance between the two arrays was measured using DGPS and the average sound speed can be calculated from the CTD measurements. Therefore, both Eq. (2) or (3) can be used to invert the current velocity.

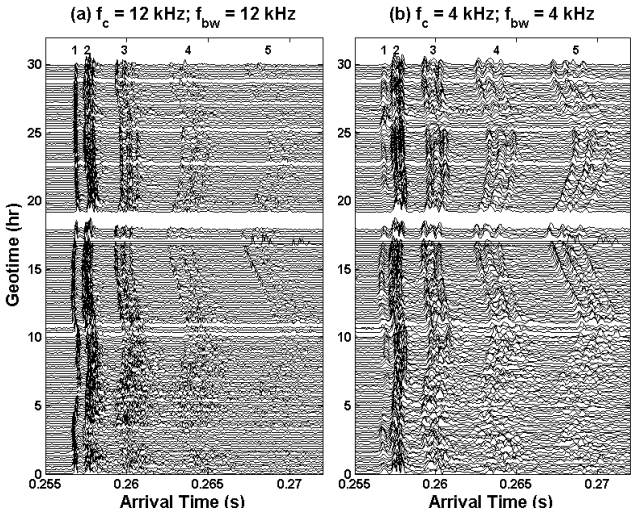

Fig. 4: Received signal amplitude versus arrival time as a function of geotime starting at 05:00:00 on September 24, 1997. Signal is from receiver channel 6 (at 2.18 m above sea floor). (a) The frequency is 12-12 kHz; (b) The frequency is 4-4 kHz.

4.2 Measurement of acoustic signal arrival time

In shallow water, the measurement of arrival time is often difficult as the acoustic rays usually interfere with each other causing indistinct separation of each peak in the group. Since HFA97 experiment provides a vertical spatial coverage of the receivers with 3 hydrophones mounted on each tripod the acoustic pressure can be represented by acoustic beam-form in relation with arrival time and grazing angle of the acoustic rays, clearly separating one peak from another. Thus to increase the accuracy of the arrival time measurements, the arrival times in this study are measured from acoustic transmission data using beamforming peak-picking technique [5]. The technique is explained in the Appendix.

Wave-induced multipath rays complicate the measurement of acoustic signals arrival times. In his study, Lewis [6] concluded that for tomography the arrival time of each group should be the very first matched filter peak arrival. In attempt to eliminate the error due to sea surface motion and scattering, the values of arrival time are averaged over the number of pings in the transmission duration [7].

Figure 5 shows beamforming diagram for different sea states (calm, intermediate, and rough) for frequencies 12-12 kHz [Fig. 5(a) to 5(c)] and 4-4 kHz [Fig. 5(d) to 5(f)]. In Fig. 5(a) to 5(c) the first spot appears at arrival time around

0.256 s representing the direct path which has a near zero arrival angle. With the combination of the bottom bounce ray, this spot is stretched to slightly away from angle zero. Note that since in the experiment the sources and receivers have been successfully synchronized, the arrival time shown in these figures represents the time for the acoustic rays to travel from the source to the receiver. For the calm sea in Fig. 5(a), there are four distinct spots correspond to Group 2 which contains four ray paths having a single sea surface interaction (see Fig. 3). The measured angle and arrival times compare well with those predicted by source-receiver waveguide geometry (3.7°, -4.3°, 4.6°, and -5.3° respectively). For the intermediate and rough sea in Fig. 5(b) and 5(c), the four deterministic ray paths are scattered by the sea surface into micro-multipaths with spread arrival angles and times, making arrival time peak-picking less accurate.

Figure 5 also clearly shows the dependency on the center frequency and bandwidth discussed above. The peaks of the Group 1 are clear for frequency 12-12 kHz while for frequency 4-4 kHz, they are more difficult to identify. The conditions for later groups are reversed. Note that for frequency 4-4 kHz, the peaks of the later arrival are still distinct even for intermediate and rough sea conditions. In Fig. 5(d) to 5(f), the four ray paths in Group 2 are not distinctly separated due to the narrow bandwidth of 4 kHz.

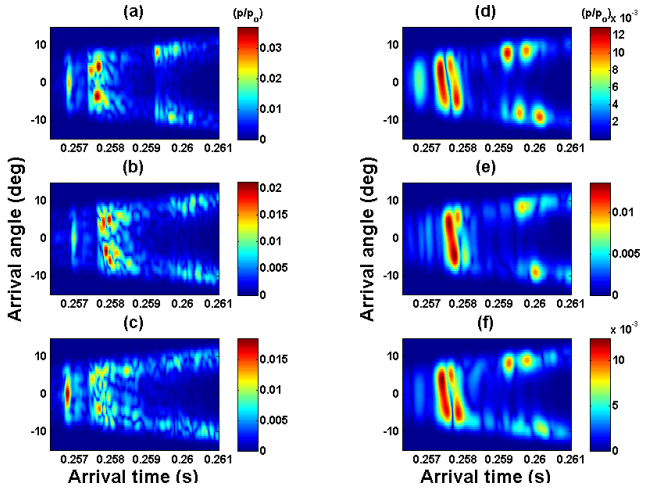

Fig. 5: Acoustic pressure beamforming diagram. (a) Data from a calm day (wind speed of 2 m/s) for f=12-12 kHz , (b) Data from an intermediate day (wind speed of 5 m/s) for f= 12-12 kHz , (c) Data from a rough day (wind speed of 12m/s) for f = 12-12 kHz, (d) Data from a calm day for f= 4-4 kHz , (e) Data from an intermediate day for f = 4-4 kHz , (c) Data from a rough day for f = 4-4 kHz.

4.3 Current estimation results

The current velocity was calculated using Eq. (2) with average sound speed C from CTD measurements and average arrival times t_{AC} and t_{CA} within each transmission.

In Fig. 6 the current estimation for 30 hr starting at 5:00am on September 24, 1997 is presented and compared with the ADCP current measurements. For Group 1, the estimated current was compared with the near bottom ADCP measurements projected in the source-receiver direction, while for later groups it was compared with the depth-averaged ADCP measurements also projected in the source-receiver direction. Figures 6(a) and 6(b) are for frequencies 12-12 kHz and 4-4 kHz, respectively. From the plots, it is clear that the tidal fluctuations are predicted accurately. Moreover, in general, for a calm sea state (after hour 10) the ocean currents can be estimated accurately using the reciprocal arrival time of all the arrival groups. The differences in amplitude might be due to the fact that the acoustic measurements give an averaged value between the source and receiver, while the ADCP is a point measurement. Rough sea states at the first 10 hr significantly increase the variation of the estimations and reduce the accuracy; however, for Group 1 with no surface interaction, the sea surface condition does not affect the current estimation.

It is noticed that better accuracy can be achieved using higher center frequency for Group 1. For later groups, lower center frequency gives better estimations. Group 1 with higher frequency and Groups 2 and 3 with lower center frequency estimate the current reasonably well even for rough sea state conditions.

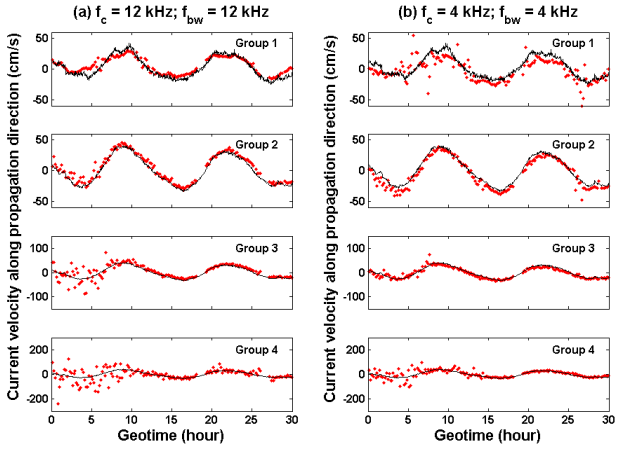

Fig. 6: Comparison between the ADCP measured current projected in the direction of acoustic propagation (solid line) and tomography inverted current for 4 arrival groups during the 30 hour observation starting at 05:00:00 on 24 September 1997. (a) The frequency is 12-12 kHz. (b) The frequency is 4-4 kHz. Note the difference in scale.

5 Summary and conclusion

In the present study, high frequency broad band acoustic tomography has been shown to successfully estimate the current using acoustic transmission data from the HFA97 experiment conducted in Delaware Bay. The experiment was carefully designed to allow a study of current tomography in shallow water regions. The results show that there is a strong dependency of the current estimations on the acoustic center frequency and bandwidth, ray paths, and ocean environment. Thus, the choice of acoustic frequency corresponding to a certain condition of the ocean environment and source-receiver configuration is crucial for acoustic current tomography in shallow water regions.

Ocean current can be estimated accurately for a calm sea state using up to the 4th ray groups reciprocal transmissions for both high and low center frequencies and bandwidths.

Appendix: The Gaussian weighted beamforming

Signal that arrives at the receiver is analyzed here as a function of geotime t_g, arrival time t_a, and arrival angle θ_a. A delay-and-sum beamforming technique capable of separating the ray paths in each group of arrivals is used to resolve and identify individual rays. Typically beamforming technique is applied to a large number of receivers to satisfy the spatial sampling requirement of $d<\lambda/2$ to avoid aliasing where λ is the acoustic wave length and d is the hydrophone spacing. In our situation, only 3 hydrophones are available, which implies an under-sampling in spatial domain. To overcome this problem the Gaussian weighting function is applied. It is an *a priori* technique based on the calculation of the ray path propagation for the HFA97 configuration and is a probabilistic estimation of the existence of beamforming pressure for all points (t_a,θ_a) [6]. Based on the geometry of the considered acoustic waveguide, the sound speed for a given couple of (t_a,θ_a) is $C_{calc}(t_a,\theta_a) = D/((t_a \cos \theta_a)$, where D is the known distance between source and receiver. This calculated sound speed implies the existence of a weighting function $W(t_a,\theta_a)$ built by comparison with a reference speed C_o as

$$W(t_a,\theta_a) = e^{-\left(\frac{C_{calc}-C_o}{\Delta C}\right)^2} \qquad (4)$$

where ΔC is the uncertainty in the sound speed. The reference sound speed C_o corresponds to the mean value of the measured sound speed during the week of the experiment. ΔC represents the approximate range between the minimum and the maximum values of the sound speed measured during the experiment and is equal to 10 m/s in our calculation. The weighted beamformed pressure p_{bg} is then obtained by multiplying the pressure p_b with the Gaussian weighting function W. Figure 7(a) represents W for an uncertainty ΔC of 10 m/s. Scales are ranging from 0 to 1 which correspond to the minimum and maximum probability of physical existence of beamformed pressure, respectively.

To demonstrate the viability of the Gaussian-weighted beamforming technique, a synthetic data were generated using ray based Bellhop model [8] to simulate HFA97 experiment. The minimum number of hydrophones to satisfy the spatial sampling requirement for HFA97 with acoustic signal center frequency of 12 kHz is 30. Figures 7(b), 7(c), and 7(d) show the beamforming results for 3 different cases: 30 hydrophones with no Gaussian weighting filter (GW), 3 hydrophones with no GW, and 3 hydrophones with GW respectively. Note the time scale difference in Fig. 7(a). The range of arrival time in Fig. 7(b), 7(c), and 7(d) lies between two dashed-lines in Fig. 7(a). Figure 7(b) shows five distinct patches which correspond to the first group and four ray paths in the second group of arrival. Figure 7(c) shows the same information with multiple false patches and side lobes at times and angles where physically do not exist considering the set up of the experiment. However, the location of peaks with the GW shown in Fig. 7(d) is identical to the case with 30 hydrophones shown in Fig. 7(b).Therefore, using the given vertical spatial coverage of the receivers, the acoustic pressure can be represented by an acoustic beam in relation with grazing angle and arrival time of acoustic rays.

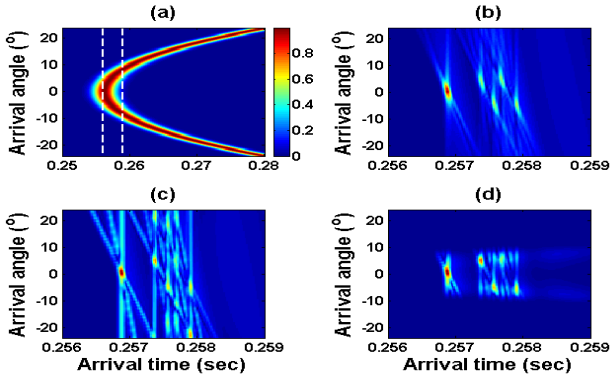

Fig. 7: (a) Gaussian weighting function (GW) with sound speed uncertainty of 10 m/s. (b) Beamforming diagram for numerically generated data for high number of hydrophones, no GW applied; (c) low number of hydrophones, no GW; (d) low number of hydrophones, GW applied. Note the time scale difference in (a). The range of arrival time in (b), (c), and (d) lies between two dashed-lines shown in (a).

Acknowledgments

The authors wish to thank Art Sundberg, Luc Lenain, Steve Forsythe, Jeremie Largeaud, and Robert Heitsenrether for their assistance in different aspects of this research. This research was supported by the Office of Naval Research and in part by the University of Delaware Sea Grant.

References

[1] Munk, W., Worcester, P.F, and Wunsch, C. *Ocean Acoustic Tomography*. Cambridge University Press, 1995.

[2] Howe, B.M., Worcester, P.F., and Spindel, "Ocean acoustic tomography: Mesoscale velocity," J. Geophys. Res., vol. 92, 3785-3865, 1987.

[3] Badiey, M., Simmen, J.A, and Forsythe, S.E., "Frequency dependence of broadband propagation in coastal regions," J. Acoust. Soc. Am. 101(6), 3361-3370, 1997.

[4] Dushaw, B.D., Worcester, P.F., Cornuelle, B.D. and Howe, B.M., "On equations for the speed of sound in seawater," J. Acoust. Soc. Am., 93, 255-275, 1993.

[5] Lenain, L., "Characteristics of broadband high frequency acoustic propagation in coastal environment", Master's thesis, University of Delaware, 2002.

[6] Lewis, J.K., "Determining tomographic arrival times based on matched filter processing: Considering the impact of ocean waves", J. Acoust. Soc. Am., 123(2), 878-886, 2008.

[7] Lewis, J.K., Rudzinsky, J., Subramaniam, S., Stein, P.J., Vandiver, A., The Kauai Group, "Model-oriented ocean tomography using higher frequency, bottom-mounted hydrophones", J. Acoust. Soc. Am., 117(6), 3539-3554, 2005.

[8] Jensen, F. B., Kuperman, W.A., Porter, M.B., and Schmidt, H., "Computational Ocean Acoustics," American Institute of Physics, New York, 1994.